ChemPhysChem

Research Article
doi.org/10.1002/cphc.202300326

Chemistry Europe
European Chemical Societies Publishing

www.chemphyschem.org

Comparison of the Ability of N-Bases to Engage in Noncovalent Bonds

Akhtam Amonov[a] and Steve Scheiner*[b]

The lone pair of the N atom is a common electron donor in noncovalent bonds. Quantum calculations examine how various aspects of the base on which the N is located affect the strength and other properties of complexes formed with Lewis acids FH, FBr, F_2Se, and F_3As that respectively encompass hydrogen, halogen, chalcogen, and pnicogen bonds. In most cases the halogen bond is the strongest, followed in order by chalcogen, hydrogen, and pnicogen. The noncovalent bond strength increases in the $sp < sp^2 < sp^3$ order of hybridization of N. Replacement of H substituents on the base by a methyl group or substituting N by C atom to which the base N is attached, strengthens the bond. The strongest bonds occur for trimethylamine and the weakest for N_2.

Introduction

There is a wealth of Lewis acid-base interactions within the universe of noncovalent bonds. Probably the most well studied and understood of this class is the H-bond (HB) AH··B where the AH acid molecule accepts a certain amount of charge from the base B. In the most common such bond, it is a lone pair of B which transfers charge into the σ*(AH) antibonding orbital of the acid.[1–8] The HB is the "display model" of sorts for a range of very similar bonds in which the bridging proton is replaced by any of a wide diversity of other atoms. Many of these variants are sometimes grouped under the umbrella sobriquet of σ-hole bonds due to a common feature in which there is a depletion of electron density along the extension of the R–A covalent bond where A refers to the H replacement. Both this density depletion and the positive charge in the molecular electrostatic potential that it causes have been dubbed a σ-hole. Each such σ-hole bond is commonly classified by the family of the A atom which contains this hole. The halogen atom X contains one such hole,[9–20] while a chalcogen Y atom would typically have two σ-holes,[21–35] one for each of its two R_2Y covalent bonds. This pattern continues with three σ-holes on the pnicogen Z atom of R_3Z,[36–42] and four for a tetrel atom T in a R_4T molecule.[28,43–52]

There has been a great deal of focused study of late that has helped to characterize each of these noncovalent bonds, and has shown a high dependency of the bond strength on the depth of the σ-hole, i.e. the positive molecular electrostatic potential (MEP) along the bond axis extension.[53] This depth is in turn heavily influenced by both the nature of the bridging A atom and any substituents R to which it is bonded. For example, as one moves down a column of the periodic table, whether halogen, chalcogen, etc, there is usually a drop in electronegativity and a rise in polarizability. Both of these trends induce a deepening in the σ-hole and thereby to a stronger bond with a base. Likewise, more powerful electron-withdrawing substituents R draw density away from A, aiding in the growth of this hole.

The emphasis in prior work has lain with developing a detailed understanding of the forces that control the strength of the Lewis acid. It is a common strategy to pair a systematic list of closely related acids, with small perturbations from one to the other, with a single base. NH_3, for example, is a common universal base used in these analyses of the comparative properties of this list of acids. But while the development of ideas concerning how various aspects of an acid affect the incipient noncovalent bond, the properties of the base are no less important and merit a similar thorough and systematic analysis.

The N atom is one of the most common electron donors in these sorts of bonds. In particular, its lone pair offers an available source of electrons, easily donated to a Lewis acid. This atom is involved in a number of different sorts of molecules. Perhaps its most common bonding environment is within the context of amines, where it is sp^3-hybridized and attached to three different H or alkyl groups. A sp^2 hybridization is common to imines, and typically involves a N=C double bond. The diazo group connects two N atoms together via a double bond. This same hybridization also occurs when the N atom is an integral part of an aromatic ring, with pyridine being a prominent example. The cyano group is a common one, and places the N in a sp environment, involved in a N≡C triple bond, placing its lone pair along this bond axis. This same hybridization is characteristic of the dinitrogen molecule with its N≡N triple bond.

It is the goal of the current work to focus on the N atom in all of its guises as the electron donor atom, so as to cover a wide spectrum of its bonding environments. This atom is considered in all three of its formal hybridizations: sp^3, sp^2 and

[a] Dr. A. Amonov
Department of Optics and Spectroscopy,
Engineering Physics Institute
Samarkand State University
140104, University blv. 15, Samarkand, Uzbekistan
[b] Prof. S. Scheiner
Department of Chemistry and Biochemistry
Utah State University
Logan, Utah 84322-0300, USA
E-mail: steve.scheiner@usu.edu

sp. The latter is achieved by consideration of N≡N, HC≡N, and MeC≡N, all of which contain N involved in a triple bond to one other atom. The sp^2 hybridization is tested in the context of double bonds to N, in molecules such as HN=NH or imines like MeN=CH_2, as well as several others. Placing the N within an aromatic framework is considered via pyridine. The sp^3 N atom bonded to three other groups arises in various amines and in H_2N–NH_2. This set of bases allows analysis of the effects of bonding the pertinent N to either another N or to C. Rather than restrict study to any one particular noncovalent bond, such as the HB, each base is paired with a selection of Lewis acids that can engage it not only in a HB, but also halogen, chalcogen, and pnicogen bonds. Altogether, the entire database comprises 60 different Lewis acid-base complexes.

Methods

Quantum chemical calculations were performed in the context of the DFT framework, applying the M06-2X functional,[54] which has been shown to be an accurate means of treating noncovalent bonds of the sort of interest here.[55–62] A polarized triple-ζ aug-cc-pVTZ basis set was chosen so as to afford a large and flexible set that can capture some of the more subtle charge rearrangements. Geometries were fully optimized and demonstrated to be true minima by vibrational frequency analysis. The Gaussian 16[63] program was used as the primary vehicle to conduct these computations.

The interaction energy E_{int} of each homodimer was calculated as the difference between the energy of the complex and the sum of the energies of the two subunits, each in the geometry they adopt within the dimer. The counterpoise procedure[64] was applied to correct basis set superposition error of E_{int}. Minima of the molecular electrostatic potential (MEP) on the $\varrho = 0.001$ au isodensity surface of each base unit were identified via the Multiwfn program.[65] Atoms in Molecules (AIM) bond paths and their associated critical points were located and their densities evaluated with the aid of the AIMAll program.[66] Natural Bond Orbital (NBO) charge transfer energies[67,68] were assessed through the aid of the NBO program incorporated into Gaussian.

Results

Consideration of the molecular electrostatic potential (MEP) surrounding each base offers a glimpse into the orientation it will adopt with reference to the Lewis acid with which it partners. The focus of the MEP of each base is the negative potential in the vicinity of the N lone pair. After the elucidation of that aspect in Section 1, each base is then allowed to pair with one of four Lewis acids, to form a dyad bound by a clearly defined noncovalent bond. The geometries and energetics of these complexes are defined in Section 2, followed in the next section by several sorts of analysis into the nature of their binding.

Monomer Properties

The MEP of each of the N-bases considered here contains a minimum roughly coinciding with a N lone pair. Some representative potentials are exhibited in Figure 1 for each of the three N hybridizations, with their minima indicated by the red regions. The value of this minimum on a $\varrho = 0.001$ au isodensity surface is reported in the first column of Table 1. The data are separated into three sections, depending upon the nominal hybridization of the N. With the exception of N_2, the minima on the N atoms of all of the bases are between −32 and −39 kcal/mol. Within each class of molecules grouped by the ostensible hybridization of the N atom, there are some trends that conform to concepts of electronegativity. For example, the replacement of a H atom by an electron-donating methyl group adds to the negative value of V_{min}, as in the change from HN=NH to MeN=NH. This step is enhanced by two such Me groups as in MeN=NMe. Another increment in this negative value occurs if the N atom to which the nucleophilic N is attached is changed to the less electronegative C, as in the comparison between MeN=NH and MeN=CH_2. The aromaticity of the pyridine ring does not change V_{min} by much, leaving it in

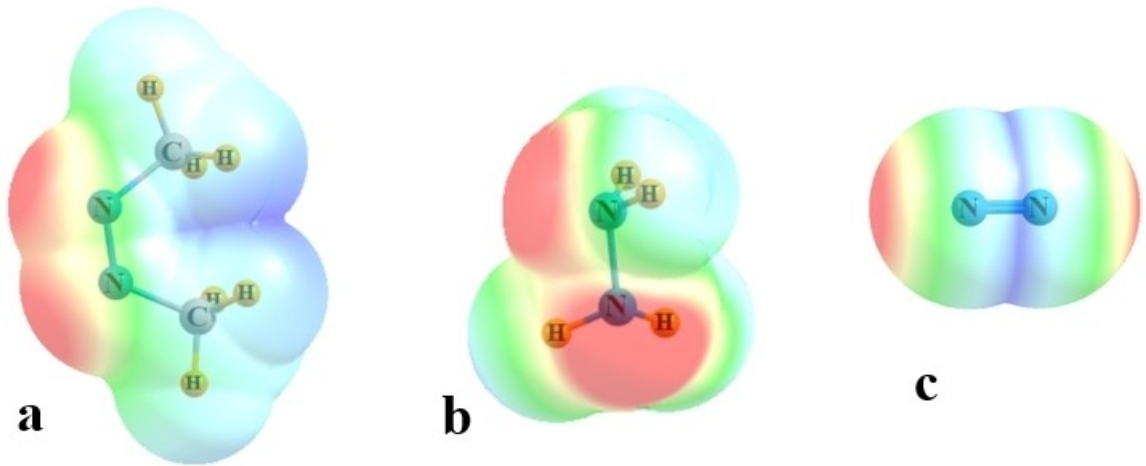

Figure 1. MEP surrounding a) MeN=NMe, b) H_2N-NH_2, and c) N≡N. Blue and red colors correspond to positive and negative regions, respectively. The extremes represented by these colors are ±30 kcal/mol in a and b, +20 and −6 kcal/mol in c.

Table 1. MEP minima on N lone pair for monomer, and interaction energy of each dyad pairing, all in kcal/mol.

	$-V_{min}$	$-E_{int}$ FH	FBr	F_2Se	F_3As
sp					
N≡N	7.9	2.06	2.37	1.94	1.49
HC≡N	32.1	7.65	7.06	6.18	4.94
MeC≡N	38.7	9.44	8.72	7.75	7.39
sp^2					
HN=NH	31.7	9.74	12.40	12.66	8.09
MeN=NH[a]	35.0	10.77	13.65	13.62	8.78
MeN=NH[a]	32.7	10.78	14.82	14.73	10.42
MeN=NMe	37.7	12.73	17.70	14.74	12.60
$HN=CH_2$	37.0	13.29	16.02	14.92	10.38
$MeN=CH_2$	35.6	14.12	19.17	16.17	11.73
C_6H_5N	36.2	14.42	18.81	16.17	11.38
sp^3					
NH_3	36.6	14.11	15.71	13.52	10.34
$H_2N\text{-}NH_2$	33.4	14.54	17.86	16.08	12.78
NH_2Me	36.5	15.80	19.98	17.72	13.03
$NHMe_2$	34.1	16.82	22.94	19.82	14.82
NMe_3	31.6	17.19	24.58	22.09	16.42

[a] bond formed to underlined N atom

the same range as $HN=CH_2$ and $MeN=CH_2$. Within the amine category in the lowest section of Table 1, there is an interesting reversal of sorts, in that each replacement of a H atom of NH_3 by a methyl group makes V_{min} slightly less negative, leaving NH_3 with the most negative minimum in this category.

Energetics and Geometries

The remaining columns of Table 1 display the interaction energy between each base and one of several different Lewis acids. FH points its proton toward the base N in a classic FH··N HB. The FBr, F_2Se, and F_3As units engage respectively in a XB, YB, and ZB with the base of the type A··N where A represents any of these heavy atoms. When comparing these various types of noncovalent bonds, in most cases the interaction energy rises in the order ZB < HB < YB < XB. Taking $MeN=CH_2$ as an example, its interaction energies are 11.73 < 14.12 < 16.17 < 19.17 kcal/mol in this same order. However, this pattern cannot be taken as a universal rule as there are several exceptions. For example, the HB is the strongest of these bonds for HC≡N and MeC≡N. Also, for MeN=NH, there is very little distinction between the XB and YB, and these two bond strengths reverse for HN=NH. Overall, there is a tendency for the bond strengths to increase in the order $sp < sp^2 < sp^3$. For example, the XB interaction energy for the sp N bases ranges between 2.4 and 8.7, while these same ranges are 12.4–19.2 for sp^2, and somewhat higher at 15.7–24.6 kcal/mol for the amines. Within any particular hybridization class, the interaction energies climb as H atoms are swapped out for electron-releasing methyl groups, or adjacent N atoms are switched to less electronegative C. Note, however, that the interaction energies correlate rather poorly with the N lone pair MEP minimum, which shows much less dependence on N hybridization or substituents. In fact, for each class of noncovalent bond, HB, XB, etc, the correlation coefficient between E_{int} and V_{min} is less than 0.5.

Each of the noncovalently bound dyads place the N atom of the base in position to bind with the relevant atom of the acid, whether H, Br, Se, or As. Several representative dyad structures are displayed in Figures 2 and 3 for the MeN=NMe and $NH_2\text{-}NH_2$

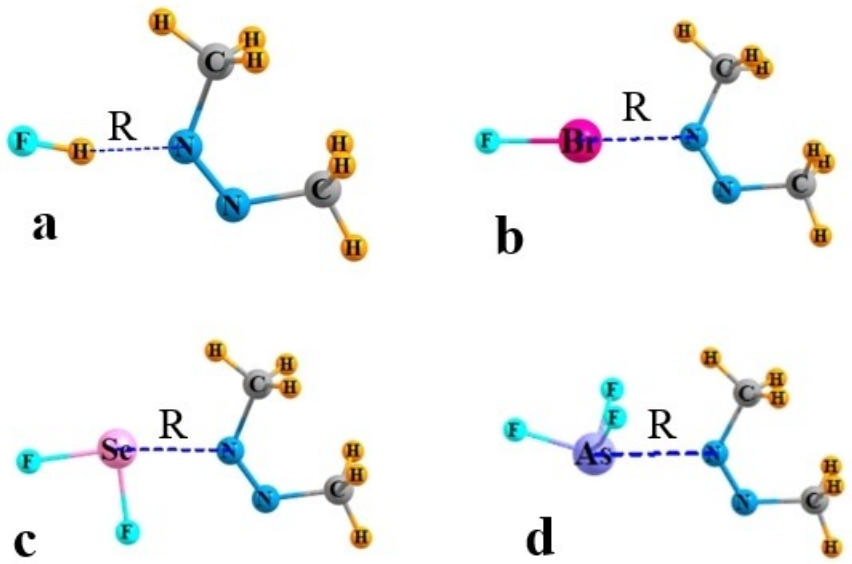

Figure 2. Optimized geometries of a) HB, b) XB, c) YB, and d) ZB dimers involving MeN=NMe.

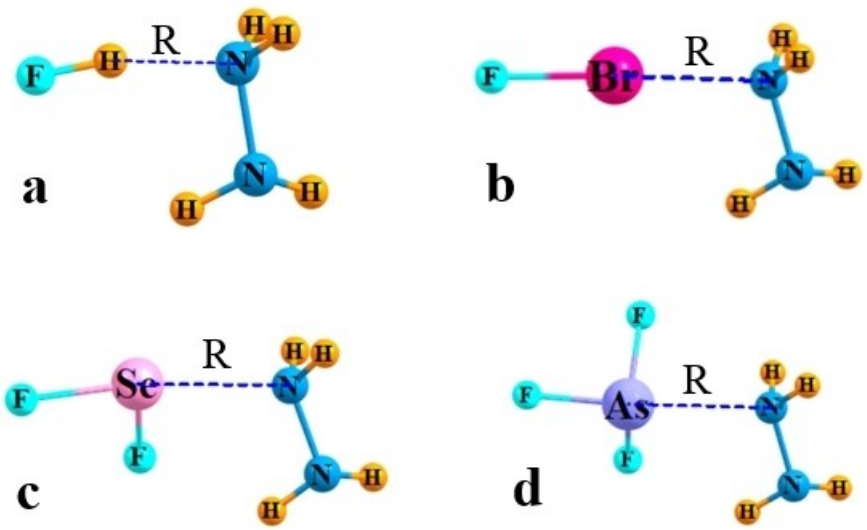

Figure 3. Optimized geometries of a) HB, b) XB, c) YB, and d) ZB dimers involving H_2N-NH_2.

bases, respectively. The intermolecular contact distance R(N··A) of each complex is presented in Table 2. The shorter distances to H are to be expected given its small size, but the trends in the other distances echo the energetics in that it is the XB that is shortest, followed in order by the YB and then the ZB. These elongations are substantial, with the HN═NH base serving as an example. The distance of its N to the Br, Se, and As atoms of the associated acids are 2.301, 2.331, and 2.728 Å. With respect to the N hybridization, the HB lengths tend to contract in the $sp > sp^2 > sp^3$ order, commensurate with the HB interaction energy growing in this same order. The patterns in the other noncovalent bond are not quite as clear, although the longer distances for sp do appear to be a general feature, even if the longer distances for sp^2 as opposed to sp^3 is not a large margin.

These intermolecular distances correlate fairly well with the interaction energies. Taking the HB, XB, YB, and ZB series separately, the correlation coefficient R^2 is equal to 0.98, 0.79, 0.81, and 0.88, respectively.

Table 2. Intermolecular A··N distance (Å) of each Lewis acid-base pair.

sp	HF	BrF	SeF_2	F_3As
N≡N	2.042	2.840	2.982	3.207
HC≡N	1.840	2.616	2.758	2.914
MeC≡N	1.793	2.564	2.681	3.013
sp^2				
HN═NH	1.751	2.301	2.331	2.728
MeN═NH	1.727	2.288	2.321	2.677
MeN═NMe	1.721	2.272	2.330	2.613
MeN═NMe	1.674	2.238	2.255	2.523
HN═CH_2	1.662	2.276	2.357	2.668
MeN═CH_2	1.641	2.231	2.324	2.543
C_6H_5N	1.630	2.239	2.323	2.535
sp^3				
NH_3	1.664	2.335	2.448	2.606
H_2N-NH_2	1.629	2.289	2.382	2.545
NH_2Me	1.618	2.273	2.314	2.493
$NHMe_2$	1.588	2.243	2.321	2.470
NMe_3	1.572	2.237	2.294	2.447

Analysis of Electron Density

As an auxiliary measure of the strength of each noncovalent bond, AIM analysis of the topology of the electron density comes at this issue from a completely different angle. Such an analysis leads to a bond path between the N of each base and the A atom of the approaching Lewis acid. A bond critical point lies along this path, roughly midway along the A··N axis. The electron density at this point, ϱ_{BCP}, offers a quantitative estimate of the strength of this noncovalent bond. The value of this density for each of the complexes is listed in Table 3 which spans the range between 0.01 and 0.08 au, comfortably in the range of noncovalent bonds of moderate strength.

The trends in ϱ_{BCP} conform to the interaction energies in a number of ways. There is a clear pattern of enlarging density in the ZB < YB < XB order, with the HBs slightly smaller than the XBs. The sp-hybridized N clearly presents smaller densities, with sp^3 slightly larger than sp^2. Changing the atom attached to the participating N from N to the less electronegative C raises ϱ_{BCP}, as does replacement of H by CH_3. Placing the N in an aromatic setting as in pyridine has little effect on its BCP density. Overall, there is a fairly good correlation between the interaction energies and the values of ϱ_{BCP}, with correlation coefficient exceeding 0.8 in all cases. Specifically, R^2 is equal to 0.92, 0.86, 0.84, and 0.93, respectively for the HB, XB, YB, and ZB series.

A common observation in the formation of noncovalent bonds of these sorts is the transfer of charge from the lone pair of the basic N to the σ*(AX) antibonding orbital corresponding to the AX bond that lies diametrically opposite to the basic N. The energetic consequence of this transfer is the NBO value of E2, the second-order perturbation energy. These values of E2

Table 3. AIM A··N bond critical point density, au.

	HF	BrF	SeF_2	F_3As
sp				
N≡N	0.0187	0.0155	0.0119	0.0079
HC≡N	0.0197	0.0266	0.0199	0.0153
MeC≡N	0.0368	0.0301	0.0237	0.0133
sp^2				
HN=NH	0.0461	0.0627	0.0581	0.0240
MeN=NH	0.0489	0.0645	0.0593	0.0270
MeN=NH	0.0508	0.0683	0.0596	0.0322
MeN=NMe	0.0571	0.0738	0.0696	0.0393
$HN=CH_2$	0.0573	0.0663	0.0550	0.0283
$MeN=CH_2$	0.0617	0.0746	0.0606	0.0378
C_6H_5N	0.0634	0.0732	0.0606	0.0385
sp^3				
NH_3	0.0584	0.0595	0.0465	0.0328
$H_2N\text{-}NH_2$	0.0649	0.0675	0.0547	0.0384
NH_2Me	0.0667	0.0697	0.0632	0.0427
$NHMe_2$	0.0727	0.0757	0.0634	0.0461
NMe_3	0.0763	0.0778	0.0682	0.0492

are reported in Table 4 for each of the dyads considered here. There are several anomalies in the NBO analysis as follows. Some dyads were treated by NBO as a single unit, so the source of the density is designated formally as a covalent N–Se or N–As bond. There are also two cases involving pyridine where the destination of the charge emanating from the N lone pair was designated an unoccupied H, Se, or As lone pair, rather than as a σ*(AF) antibonding orbital. These exceptions are indicated by the appropriate footnotes in Table 4.

These NBO indicators of bond strength conform to the patterns followed by the quantities described above. There is a clear increasing trend from ZB to YB to XB, with the HB quantities generally intermediate between these extremes. The exceptions are the sp N atoms of HC≡N and MeC≡N where the HB quantity is the largest of all. By and large, E2 rises in the order $sp < sp^2 < sp^3$, with the exception of a particularly large value for pyridine, which clearly exceeds the other sp^2 bases. There is a modest correlation between energetics and E2. The correlation coefficient between these two quantities is equal to 0.84, 0.90, 0.78, and 0.45 for the HB, XB, YB, and ZB, respectively.

Table 4. NBO values of E2 (kcal/mol) for transfer from N lone pair to σ*(AF) antibonding orbital for AF bond lying opposite the A··N direction.

	HF	BrF	SeF_2	F_3As
sp				
N≡N	4.13	5.19	2.36	0.51
HC≡N	12.95	11.55	5.34	1.78
MeC≡N	16.67	14.57	7.66	1.39[a]
sp^2				
HN=NH	23.66	42.97	28.19	4.99
MeN=NH	26.39	45.59	29.36	6.46
MeN=NH	25.45	48.35	27.72	7.55
MeN=NMe	31.60	54.96	53.71[b]	10.27
$HN=CH_2$	34.23	50.49	29.47	7.34
$MeN=CH_2$	36.84	59.92	48.66[b]	10.85
C_6H_5N	56.97[c]	59.22	56.86[c]	25.96[c]
sp^3				
NH_3	39.00	48.60	24.83	9.78
$H_2N\text{-}NH_2$	41.16	54.58	28.86	11.47
NH_2Me	42.86	58.42	54.01[b]	13.10
$NHMe_2$	44.63	62.28	55.77[b]	33.14[b]
NMe_3	43.62	60.51	56.41[b]	12.91

[a] source is combined N lone pair + N=C bond; [b] source is N–Se/As bond as NBO treats as single unit; [c] destination is H/Se/As lone pair

While useful as a means to focus on the transfer between two particular orbitals, it is enlightening to examine the total picture of density shifts that accompany the formation of each of these noncovalent bonds. These shifts encompass both the transfer from one subunit to the other and the internal polarizations within each monomer. These density shifts are portrayed in Figure 4 for the halogen bonds between FBr and each of the N_2H_n units where n = 0, 2, and 4; i.e. sp, sp^2 and sp^3-hybridized N. The purple regions denote gains of density resulting from the dimerization whereas depletions are indicated in green.

The patterns in Figure 4 are common to the shifts in most XBs that have been examined in this manner. There is a large purple region of gain roughly midway between the Br and N atoms, indicative of the charge buildup signifying the creation of a new noncovalent bond. This purple region is flanked on its right by a density depletion from the N lone pair, caused in part by the transfer across to the acid, as well as internal polarizations within the base unit. There is also a green area directly to the right of Br, arising in large measure from the internal

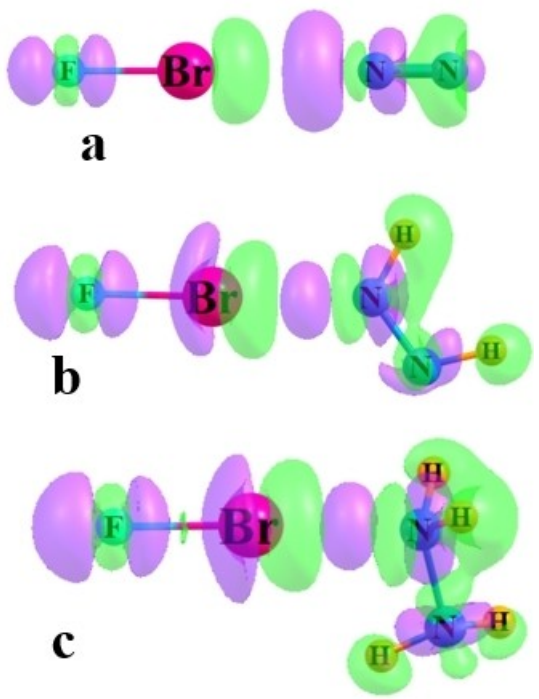

Figure 4. Electron density shifts accompanying formation of XB complexes of FBr with a) N≡N, b) HN=NH, and c) $H_2N\text{–}NH_2$. Purple and green regions indicate gain and loss of density, respectively. Contours shown are ±0.0005 au in a and ±0.0020 au in b and c.

polarization of the FBr subunit. It should be mentioned finally that the contours depicted in Figure 4a were ± 0.0005 au, as compared to ± 0.0020 au for 4b and 4c, since the much weaker binding of N_2 causes smaller density shifts.

Conclusions

All of the N bases described here are capable of acting as electron donors in the context of a HB, XB, YB, or ZB. A sp hybridization of the N in bases where it engages in an internal triple bond, as in N_2, HCN, or MeCN, results in a somewhat weaker binding than when a sp^2 N forms a double bond to one substituent, which is in turn weaker than the sp^3 hybridization of a N bound to three separate substituents by single covalent bonds. Substituents that can be thought of as electron-releasing tend to strengthen the noncovalent bond of the N lone pair with a Lewis acid, even if not always mirrored by V_{min}. Replacement of H by CH_3 is one example of this effect, as is the switching of a N atom attached to the binding N to a less electronegative C. Placing a sp^2 N within an aromatic system as in pyridine has only a small strengthening effect on the noncovalent bond it can form. Of the set of bases examined here, N_2 forms the weakest bonds, between 1.5 and 2.5 kcal/mol, and NMe_3 the strongest, in the 16–25 kcal/mol range. There is a general tendency for the halogen bonds to be the strongest category, followed by chalcogen, hydrogen, and then pnicogen bonds as the weakest group.

Acknowledgements

This material is based upon work supported by the National Science Foundation under Grant No. 1954310.

Conflict of Interest

The authors declare no conflict of interest.

Data Availability Statement

The data that support the findings of this study are available from the corresponding author upon reasonable request.

Keywords: hydrogen bond · halogen bond · pnicogen bond · chalcogen bond · density functional calculations

[1] G. C. Pimentel, A. L. McClellan, *The Hydrogen Bond*, Freeman, San Francisco, **1960**.
[2] S. Scheiner, L. Wang, *J. Am. Chem. Soc.* **1993**, *115*, 1958–1963.
[3] M. D. Joesten, L. J. Schaad, *Hydrogen Bonding*, Marcel Dekker, New York, **1974**.
[4] S. Cybulski, S. Scheiner, *J. Am. Chem. Soc.* **1987**, *109*, 4199–4206.
[5] G. R. Desiraju, T. Steiner, *The Weak Hydrogen Bond in Structural Chemistry and Biology*, Oxford, New York, **1999**.
[6] G. A. Jeffrey, W. Saenger, *Hydrogen Bonding in Biological Structures*, Springer-Verlag, Berlin, **1991**.
[7] G. Gilli, P. Gilli, *The Nature of the Hydrogen Bond*, Oxford University Press, Oxford, UK, **2009**.
[8] S. Horowitz, L. M. A. Dirk, J. D. Yesselman, J. S. Nimtz, U. Adhikari, R. A. Mehl, S. Scheiner, R. L. Houtz, H. M. Al-Hashimi, R. C. Trievel, *J. Am. Chem. Soc.* **2013**, *135*, 15536–15548.
[9] D. F. Mertsalov, R. M. Gomila, V. P. Zaytsev, M. S. Grigoriev, E. V. Nikitina, F. I. Zubkov, A. Frontera, *Cryst.* **2021**, *11*, 1406.
[10] J. E. Del Bene, I. Alkorta, J. Elguero, *Chem. Phys. Lett.* **2020**, *761*, 137916.
[11] M. Palusiak, S. J. Grabowski, *Struct. Chem.* **2008**, *19*, 5–11.
[12] S. J. Grabowski, *J. Phys. Chem. A.* **2011**, *115*, 12340–12347.
[13] S. Scheiner, S. Hunter, *ChemPhysChem.* **2022**, *23*, e202200011.
[14] J. S. Murray, P. Politzer, *ChemPhysChem.* **2021**, *22*, 1201–1207.
[15] A. V. Cunha, R. W. A. Havenith, J. van Gog, F. De Vleeschouwer, F. De Proft, W. Herrebout, *Molecules.* **2023**, *28*, 772.
[16] A. Bauzá, A. Frontera, *Theor. Chem. Acc.* **2017**, *136*, 37.
[17] G. Cavallo, P. Metrangolo, R. Milani, T. Pilati, A. Priimagi, G. Resnati, G. Terraneo, *Chem. Rev.* **2016**, *116*, 2478–2601.
[18] S. Scheiner, *CrystEngComm.* **2013**, *15*, 3119–3124.
[19] T. Clark, M. Hennemann, J. S. Murray, P. Politzer, *J. Mol. Model.* **2007**, *13*, 291–296.
[20] A. J. Taylor, A. Docker, P. D. Beer, *Chem. Asian J.* **2023**, *18*, e202201170.
[21] G. R. Desiraju, V. Nalini, *J. Mater. Chem.* **1991**, *1*, 201–203.
[22] M. Iwaoka, S. Tomoda, *J. Am. Chem. Soc.* **1994**, *116*, 2557–2561.
[23] O. Carugo, *Biol. Chem.* **1999**, *380*, 495–498.
[24] R. J. Fick, G. M. Kroner, B. Nepal, R. Magnani, S. Horowitz, R. L. Houtz, S. Scheiner, R. C. Trievel, *ACS Chem. Biol.* **2016**, *11*, 748–754.
[25] A. J. Mukherjee, S. S. Zade, H. B. Singh, R. B. Sunoj, *Chem. Rev.* **2010**, *110*, 4357–4416.
[26] C. B. Aakeroy, D. L. Bryce, G. R. Desiraju, A. Frontera, A. C. Legon, F. Nicotra, K. Rissanen, S. Scheiner, G. Terraneo, P. Metrangolo, G. Resnati in *Definition of the chalcogen bond (IUPAC Recommendations 2019), Vol. 91* (Ed.Eds.: Editor), City, **2019**, pp.1889.
[27] J. Fanfrlík, A. Přáda, Z. Padělková, A. Pecina, J. Macháček, M. Lepšík, J. Holub, A. Růžička, D. Hnyk, P. Hobza, *Angew. Chem. Int. Ed.* **2014**, *53*, 10139–10142.
[28] A. C. Legon, *Phys. Chem. Chem. Phys.* **2017**, *19*, 14884–14896.
[29] I. Alkorta, J. Elguero, J. E. Del Bene, *ChemPhysChem.* **2018**, *19*, 1886–1894.
[30] C. Trujillo, I. Rozas, J. Elguero, I. Alkorta, G. Sánchez-Sanz, *Phys. Chem. Chem. Phys.* **2019**, *21*, 23645–23650.
[31] S. Scheiner, J. Lu, *Chem. Eur. J.* **2018**, *24*, 8167–8177.
[32] O. Carugo, G. Resnati, P. Metrangolo, *ACS Chem. Biol.* **2021**, *16*, 1622–1627.
[33] S. Scheiner, *CrystEngComm.* **2021**, *23*, 6821–6837.
[34] H. S. Biswal, A. K. Sahu, B. Galmés, A. Frontera, D. Chopra, *ChemBioChem.* **2022**, *23*, e202100498.
[35] K. T. Mahmudov, A. V. Gurbanov, V. A. Aliyeva, M. F. C. Guedes da Silva, G. Resnati, A. J. L. Pombeiro, *Coord. Chem. Rev.* **2022**, *464*, 214556.
[36] J. E. Del Bene, I. Alkorta, G. Sanchez-Sanz, J. Elguero, *J. Phys. Chem. A.* **2011**, *115*, 13724–13731.
[37] A. Bauzá, D. Quiñonero, P. M. Deyà, A. Frontera, *Phys. Chem. Chem. Phys.* **2012**, *14*, 14061–14066.
[38] Q.-Z. Li, R. Li, X.-F. Liu, W.-Z. Li, J.-B. Cheng, *ChemPhysChem.* **2012**, *13*, 1205–1212.
[39] G. Sánchez-Sanz, I. Alkorta, C. Trujillo, J. Elguero, *ChemPhysChem.* **2013**, *14*, 1656–1665.
[40] D. Setiawan, E. Kraka, D. Cremer, *J. Phys. Chem. A.* **2015**, *119*, 1642–1656.
[41] M. D. Esrafili, F. Mohammadian-Sabet, E. Vessally, *Mol. Phys.* **2016**, *114*, 2115–2122.
[42] S. Sarkar, M. S. Pavan, T. N. Guru Row, *Phys. Chem. Chem. Phys.* **2015**, *17*, 2330–2334.
[43] D. Mani, E. Arunan, *Phys. Chem. Chem. Phys.* **2013**, *15*, 14377–14383.
[44] D. Mani, E. Arunan, *J. Phys. Chem. A.* **2014**, *118*, 10081–10089.
[45] P. R. Varadwaj, A. Varadwaj, H. M. Marques, K. Yamashita, *CrystEngComm.* **2023**, *25*, 1411–1423.
[46] S. A. Southern, T. Nag, V. Kumar, M. Triglav, K. Levin, D. L. Bryce, *J. Phys. Chem. C.* **2022**, *126*, 851–865.
[47] S. A. C. McDowell, N. Liu, Q. Li, *Mol. Phys.* **2022**, *120*, e2111374.
[48] S. J. Grabowski, *Cryst.* **2022**, *12*, 112.
[49] A. Grabarz, M. Michalczyk, W. Zierkiewicz, S. Scheiner, *ChemPhysChem.* **2020**, *21*, 1934–1944.
[50] W. Zierkiewicz, M. Michalczyk, R. Wysokiński, S. Scheiner, *Molecules.* **2019**, *24*, 376.

[51] C. Trujillo, I. Alkorta, J. Elguero, G. Sánchez-Sanz, *Molecules.* **2019**, *24*, 308.
[52] S. J. Grabowski, *Struct. Chem.* **2019**, *30*, 1141–1152.
[53] S. J. Grabowski, W. A. Sokalski, *ChemPhysChem* **2017**, *18*, 1569–1577.
[54] Y. Zhao, D. G. Truhlar, *Theor. Chem. Acc.* **2008**, *120*, 215–241.
[55] S. Karthikeyan, V. Ramanathan, B. K. Mishra, *J. Phys. Chem. A* **2013**, *117*, 6687–6694.
[56] K. Kříž, J. Řezáč, *Phys. Chem. Chem. Phys.* **2022**, *24*, 14794–14804.
[57] A. D. Boese, *ChemPhysChem.* **2015**, *16*, 978–985.
[58] S. Kozuch, J. M. L. Martin, *J. Chem. Theory Comput.* **2013**, *9*, 1918–1931.
[59] M. Walker, A. J. A. Harvey, A. Sen, C. E. H. Dessent, *J. Phys. Chem. A* **2013**, *117*, 12590–12600.
[60] K. S. Thanthiriwatte, E. G. Hohenstein, L. A. Burns, C. D. Sherrill, *J. Chem. Theory Comput.* **2011**, *7*, 88–96.
[61] R. Podeszwa, K. Szalewicz, *J. Chem. Phys.* **2012**, *136*, 161102.
[62] M. S. Liao, Y. Lu, S. Scheiner, *J. Comput. Chem.* **2003**, *24*, 623–631.
[63] Gaussian 16 (Rev. C.01), M. J. Frisch, G. W. Trucks, H. B. Schlegel, G. E. Scuseria, M. A. Robb, J. R. Cheeseman, G. Scalmani, V. Barone, G. A. Petersson, H. Nakatsuji, X. Li, M. Caricato, A. V. Marenich, J. Bloino, B. G. Janesko, R. Gomperts, B. Mennucci, H. P. Hratchian, J. V. Ortiz, A. F. Izmaylov, J. L. Sonnenberg, D. Williams-Young, F. Ding, F. Lipparini, F. Egidi, J. Goings, B. Peng, A. Petrone, T. Henderson, D. Ranasinghe, V. G. Zakrzewski, J. Gao, N. Rega, G. Zheng, W. Liang, M. Hada, M. Ehara, K. Toyota, R. Fukuda, J. Hasegawa, M. Ishida, T. Nakajima, Y. Honda, O. Kitao, H. Nakai, T. Vreven, K. Throssell, J. A. Montgomery Jr., J. E. Peralta, F. Ogliaro, M. J. Bearpark, J. J. Heyd, E. N. Brothers, K. N. Kudin, V. N. Staroverov, T. A. Keith, R. Kobayashi, J. Normand, K. Raghavachari, A. P. Rendell, J. C. Burant, S. S. Iyengar, J. Tomasi, M. Cossi, J. M. Millam, M. Klene, C. Adamo, R. Cammi, J. W. Ochterski, R. L. Martin, K. Morokuma, O. Farkas, J. B. Foresman, D. J. Fox, Wallingford, CT, **2016**.
[64] S. F. Boys, F. Bernardi, *Mol. Phys.* **1970**, *19*, 553–566.
[65] T. Lu, F. Chen, *J. Comput. Chem.* **2012**, *33*, 580–592.
[66] T. A. Keith, AIMAll, TK Gristmill Software, Overland Park KS, **2013**.
[67] A. E. Reed, F. Weinhold, L. A. Curtiss, D. J. Pochatko, *J. Chem. Phys.* **1986**, *84*, 5687–5705.
[68] A. E. Reed, L. A. Curtiss, F. Weinhold, *Chem. Rev.* **1988**, *88*, 899–926.

Manuscript received: May 4, 2023
Revised manuscript received: May 26, 2023
Accepted manuscript online: June 2, 2023
Version of record online: June 16, 2023